Contents lists available at ScienceDirect

Journal of the Mechanics and Physics of Solids

journal homepage: www.elsevier.com/locate/jmps

Strain-engineered particle diffusion in uniaxially deformed polymer networks

Jiabin Liu, Shaoting Lin *

Department of Mechanical Engineering, Michigan State University, East Lansing, MI, USA

ARTICLE INFO

Keywords:
Nonlinear elasticity
Particle diffusion
Hydrogel
Polymer networks

ABSTRACT

Precise control of particle diffusion is highly valuable in diverse modern technologies. Traditional methods for regulating particle diffusion are often limited by inherent properties of liquid medium. This study explores mechanical deformation as a new design space to engineer particle diffusion in stretchable soft materials. Combining experimental and theoretical analyses, we discover that particle diffusivity in a uniaxially deformed polymer network is governed by two dimensionless parameters: the ratio of particle size to the polymer network's mesh size and the stretch ratio applied to the polymer network. We further demonstrate a transition in the relationship between particle diffusivity and stretch ratio, characterized by a monotonic decrease for small particles and a non-monotonic trend for large particles. This transition is attributed to the synergistic effects involving geometric transformation of the deformed polymer network and energy modulation of the stretched polymer chains. This work introduces a new mechanism for controlling particle diffusivity in polymeric materials and establishes a theoretical foundation for developing previously inaccessible transport-based technologies.

1. Introduction

The ability to precisely control particle diffusion holds great promise across diverse modern applications. In the field of medicine, for example, it is essential for drug carriers to release therapeutic agents at a controlled rate on the target site, optimizing therapeutic efficacy and minimizing side effects (Li and Mooney, 2016). In the context of electric vehicles, fine-tuning of lithium-ion diffusion plays a vital role in enhancing battery efficiency and lifespan (Kim et al., 2019). Furthermore, in environmental engineering, strategic control of particle diffusion (Raju et al., 2020) is critical for improving the effectiveness of pollution detection (Lin et al., 2019) and optimizing the efficiency of pollution removal (Zhang et al., 2014).

Traditionally, the dynamics of particle diffusion in liquid or gas adhere to Brownian motion (Poling et al., 2001), following the classical Stokes-Einstein equation $D = (k_B T)/(3\pi\eta d)$ (Einstein, 1905), where D is the particle diffusivity, k_B is the Boltzmann constant, T is the absolute temperature in Kelvin, η is the medium viscosity, and d is the particle diameter. In scenarios where medium properties (i.e., temperature and viscosity) remain constant, traditional approaches face challenges due to limited controllability and adaptivity in tuning particle diffusivity. In contrast, leveraging mechanical deformation of a stretchable polymeric medium to control particle diffusion offers inherent advantages. Firstly, the utilization of the polymer network introduces a larger design space (Ahmed, 2015; Xiang et al., 2018), such as the stiffness of polymer chains and the mesh size of the polymer networks. For instance, adjusting the

* Corresponding author.
E-mail address: linshaot@msu.edu (S. Lin).

https://doi.org/10.1016/j.jmps.2024.105732
Received 15 January 2024; Received in revised form 23 May 2024; Accepted 6 June 2024

stiffness of polymer chains impacts the resistance encountered by particles, and the mesh size of the polymer networks can be tailored to enable the selectivity of particles of different sizes. Secondly, employing mechanical deformation allows real-time and on-demand regulation of particle diffusion (Zhang et al., 2016). For example, adjusting the magnitude and duration of external forces facilitates real-time and on-demand tuning of particle diffusivity, while manipulating the direction of deformation customizes the diffusion path of particles.

While the influence of mechanical deformation on particle diffusivity has been investigated in biological tissues (Schwartz et al., 2022) and synthetic hydrogels (Lin et al., 2016; Zhao et al., 2011), the underlying mechano-transport mechanism remains inadequately understood. Existing understanding of strain-dependent diffusivity in hydrogels has been mainly attributed to the strain-induced deformations in microstructures (Bouklas and Huang, 2012; Liu et al., 2019; Sun et al., 2019; Yang et al., 2019), such as the size of polymer meshes, the connectivity of pores, and the tortuosity of diffusion pathways. For example, ultrasound was employed to expand the mesh size of self-healing ionically crosslinked hydrogel to enhance particle diffusion (Huebsch et al., 2014). Moreover, studies have focused on applying mechanical deformation to either disrupt polymer networks (Long and Hui, 2016) or deform nanoparticles (Anselmo and Mitragotri, 2017), thereby enhancing the diffusion process. For instance, a stretch-triggered drug delivery system (Wang et al., 2017) harnessed the crack propagation of the polymer network induced by mechanical deformation to augment drug release. Despite these efforts, current research has primarily focused on manipulating microstructural changes in polymer networks, while the impact of strain-induced changes on the elastic energy of polymer chains experienced by particles during their motion remains largely unexplored.

In this paper, we systematically investigate the impact of mechanical deformation on particle diffusion in stretchable soft materials, specifically focusing on diffusion under controlled uniaxial tensile load. We perform fluorescence recovery after photobleaching (FRAP) experiments on uniaxially stretched hydrogels to experimentally study how uniaxial stretch ratios affect the diffusivity of particles with different sizes. Our experimental findings reveal an intriguing transition in the relationship between particle diffusivity and stretch ratio, characterized by a monotonic decrease for small particles and a non-monotonic trend for large particles. To explain the experimental observations, we develop a cross-scale mechano-transport theory that integrates the nonlinear deformation of hydrogel, the entropic energy of polymer chains, and the hopping diffusion of particles. Our theory reveals that particle diffusivity in a stretchable polymer network is governed by two dimensionless parameters: the ratio of particle size to the polymer network's mesh size and the stretch ratio applied to the polymer network. Through combined experimental and theoretical analyses, we further delve into the synergistic effects of the geometric transformation of the polymer networks and the energy modulation of the polymer chains. This work not only provides the knowledge of mechano-transport mechanism pertinent to a broad range of biological and synthetic soft materials, but also lays a theoretical foundation for developing previously inaccessible transport-based technologies.

The remaining part of the paper is organized as follows. In Section 2, we elucidate the working principle of the proposed mechano-transport mechanism. In Section 3, we provide the experimental details on material synthesis and FRAP characterization, and discuss experimental results. In Section 4, we formulate the cross-scale mechano-transport theory that establishes the relationship between the bulk deformation of hydrogel and the diffusivity of particles. In Section 5, we discuss a specific case focusing on particle diffusion in a

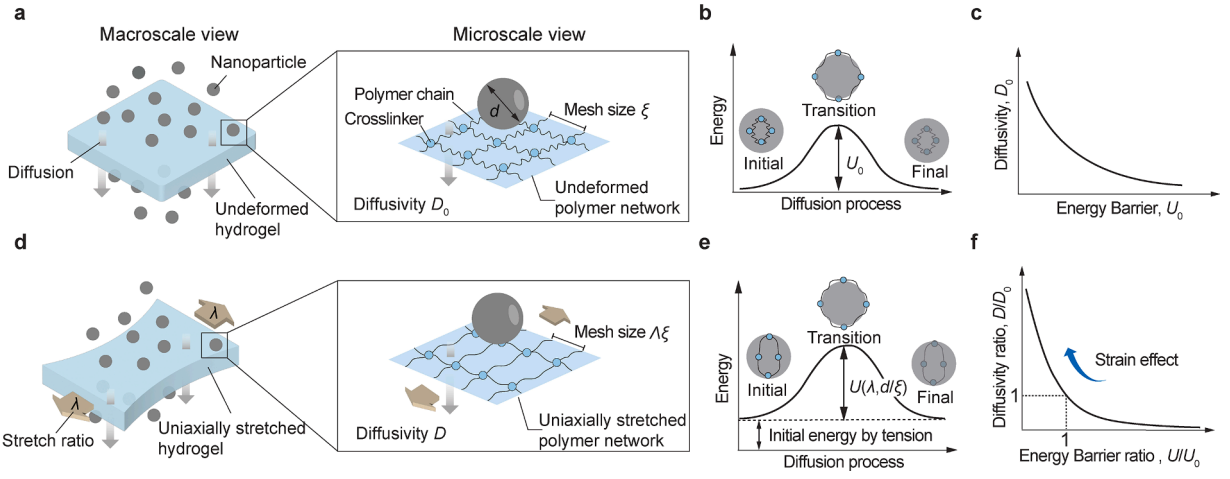


Fig. 1. Working principle of strain-engineered particle diffusion in stretchable hydrogel. (a) Schematic illustration of particles diffusing through an undeformed hydrogel. D_0 denotes the particle diffusivity in the undeformed polymer network. ξ denotes the mesh size of the polymer network, d is the diameter of the particles. (b) The diffusion of large particles in an undeformed hydrogel is governed by the energy barrier U_0 for deforming polymer chains. (c) D_0 is correlated with the energy barrier U_0 required for particle diffusion from the initial stage transition to the final stage. (d) Schematic illustration of particles diffusing through hydrogels under uniaxial tension. D represents the particle diffusivity in the deformed polymer network. Λ denotes the stretch ratio of polymer chains, which is correlated with stretch ratio λ. (e) The energy barrier U for particle diffusion through the deformed polymer network is governed by the synergy of the geometric transformation of the polymer network and the energy modulation of the polymer chains. U is a function of the stretch ratio λ and the ratio of particle diameter d to mesh size ξ. (f) Due to the strain effect of polymer networks, the diffusivity can be tuned by the energy barrier required for particle diffusion.

polymeric medium under uniaxial tension. In Section 6, we compare the experimental results with the theoretical results, focusing on how particle diffusivity varies with particle size in hydrogel under controlled uniaxial tension. In Section 7, we provide concluding remarks on this work and future perspectives for subsequent research.

2. Working principle

Fig. 1 schematically illustrates the working principle of strain-engineered particle diffusion in stretchable hydrogel. The essential idea is to modulate the particle diffusion through polymer networks by leveraging the mechanical deformation of the stretchable hydrogel. The deformation of the hydrogel leads to both the geometric transformation of the polymer network and the energy modulation of the polymer chains, which synergistically modulates the energy barrier required for particle diffusion. As shown in Fig. 1a, when large particles with a controlled diameter d diffuse through an undeformed hydrogel (from a macroscale view), the particles need to pass through multiple layers of polymer networks, which have a uniform shape with a mesh size ξ (from a microscale view). For large particles passing through each layer of the undeformed polymer network, the particles need to overcome an energy barrier U_0 to transition from the initial stage to the final stage (Fig. 1b). The energy barrier U_0, which is related to the elastic energy of polymer chains, determines the diffusion process of large particles. As shown in Fig. 1c, the particle diffusivity D_0 is a function of the energy barrier U_0, which decreases exponentially as the energy barrier U_0 increases. In contrast, as illustrated in Fig. 1d, when the hydrogel is subjected to mechanical deformation (from a macroscale view), the polymer networks undergo geometric transformation, and each polymer chain transits from a relaxed state to a stretched state with a stretch ratio Λ (from a microscale view). These two factors jointly modulate the energy barrier for particles passing through the polymer network. Consequently, the energy barrier U is a function of the stretch ratio λ and the ratio of particle diameter d to mesh size ξ (Fig. 1e). For example, if the energy barrier in the deformed polymer network is lower than that in the undeformed polymer network, the particle diffusivity is enhanced due to the strain effect (Fig. 1f).

3. Experiment method and result

3.1. Sample preparation

We synthesized a particle-hydrogel system to rigorously study the mechano-transport mechanism in soft materials. The particle-hydrogel system contains a single-network polyacrylamide (PAAm) hydrogel as the polymeric medium with a controlled mesh size ξ, and FITC-dextran (Sigma 46944, 46945, FD150S) molecules as the fluorescence particles with controlled diameters d, which can be estimated based on the molecular weight of the FITC-dextran molecules (i.e., 4 kDa, 70 kDa, and 150 kDa). To synthesize the PAAm

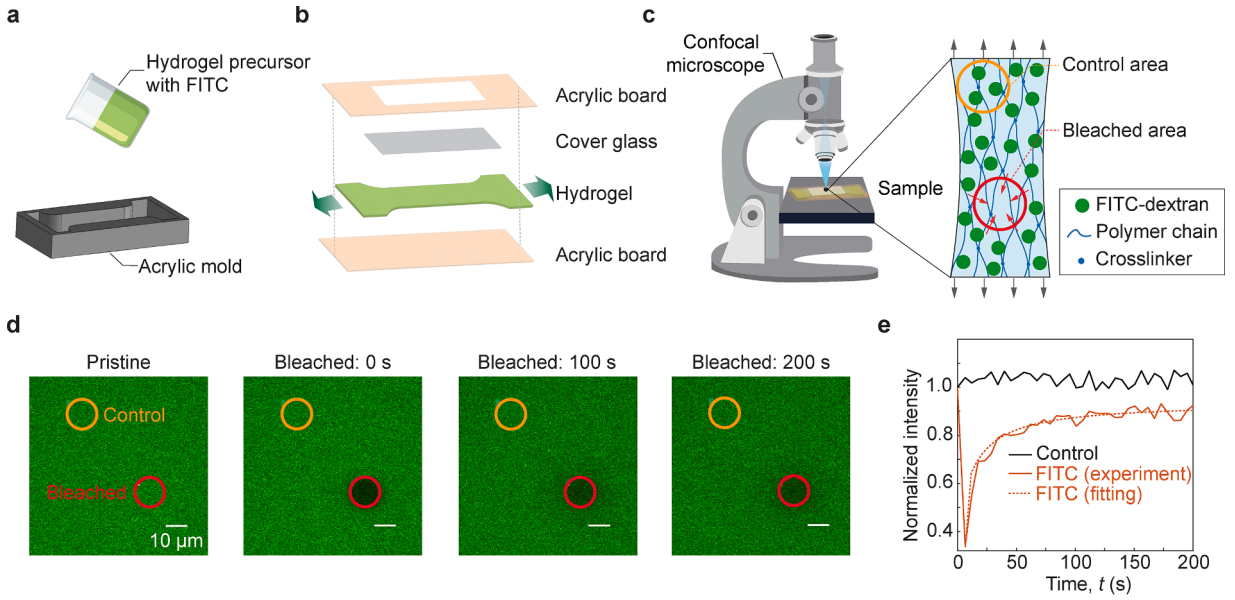


Fig. 2. Setup for sample preparation and FRAP characterization. (a) Schematic illustration of preparing the dog-bone-shaped hydrogel sample embedded with FITC molecules. (b) The pre-stretched hydrogel sample is assembled between two acrylic sheets and one cover glass for the subsequent FRAP characterization. (c) The assembled hydrogel sample is placed under a confocal microscope for FRAP characterization, during which the FITC molecules migrate into the photobleached area. (d) Representative confocal image sequences throughout the FRAP characterization. The red circle marks the region subjected to photobleaching for measurements, whereas the yellow circle marks the region without photobleaching, serving as the control. (e) Plot of the normalized intensity versus time of the regions with and without photobleaching. The dotted line denotes the fitting curve for extracting the FITC diffusivity.

hydrogel embedded with fluorescent FITC-dextran molecules, we started with a 10 mL hydrogel precursor solution, which was prepared by mixing 0.8 g acrylamide (AAm, Sigma A8887) as the monomer, 500 μL of 0.23 wt% N,N'-Methylenebisacrylamide (MBAA, Sigma 146,072) as the crosslinker, 100 μL of 0.1 M ammonium persulfate (APS, Sigma A3678) as the thermal initiator, 10 μL N,N,N',N'-tetramethylethylenediamine (TEMED, Sigma T9281) as the accelerator, and 10 mg FITC-dextran as the fluorescence particles in 9.2 mL of deionized water. Thereafter, the precursor was vortexed by a centrifugal mixer (Kr-100, THINKY) for 30 s and then poured into a dog-bone-shaped acrylic mold sealed with an acrylic cover (Fig. 2a). The acrylic mold has dimensions with a fixed width of 25 mm, a fixed thickness of 3 mm, and varying lengths of 75 mm, 37.5 mm, 25 mm, 18.5 mm, 15 mm, and 11 mm. Subsequently, the molds containing the precursor solution were placed on a 55 °C hot plate for 0.5 h until curing, fully covered with foil to prevent light exposure, which can cause photobleaching and degradation of fluorescent molecules that would adversely affect experimental results. After curing, each sample was stretched to 75 mm, yielding controlled uniaxial stretch ratios of 1, 2, 3, 4, 5, and 7, respectively. The stretched sample was then assembled on an acrylic sheet (25 mm × 75 mm × 15 mm), covered with microscope cover slides for the subsequent fluorescence recovery after photobleaching (FRAP) characterization (Fig. 2b).

3.2. FRAP experiment

Fluorescence recovery after photobleaching (FRAP) is a microscopic technique used to study the diffusion and interactions of macromolecules. This technique utilizes a high-intensity laser to bleach the fluorescent molecules in a targeted area and continuously records the intensity of the bleached region to measure two-dimensional lateral diffusion (Lorén et al., 2015). In the experiment, we used a confocal laser scanning microscope (Spectral-based Olympus FluoView) with a 20X magnification objective and a 488 nm laser (10 mW). As shown in Fig. 2c, the pre-stretched hydrogel was placed on the microscope stage, followed by a powerful laser that was employed to photobleach the central region for three seconds. To optimize the image quality and minimize the photodamage effect, the size of the bleached area and the scanning laser power were adjusted for each FITC particle. For the 4 kDa FITC-dextran, a circular region with a diameter of 24.8 μm was subjected to bleaching. After the bleaching process, the bleached area was recorded every second for one minute using a scanning laser with 0.5 % power. Similarly, for the 70 kDa and 150 kDa FITC-dextran, circular regions with diameters of 12.4 μm and 6.2 μm were subjected to bleaching, respectively. These two bleaching processes were followed by scanning every five seconds for three minutes using a laser with 0.5 % power. As shown in Fig. 2d, the bleached area temporarily turned dark during the photobleaching process and gradually regained intensity over time. In contrast, a control area was recorded simultaneously, serving as a baseline to monitor intensity changes without bleaching. Fig. 2e shows the representative curves in the plot of normalized intensity as a function of time in both the bleached and control areas. To determine the diffusivity from the measured intensity over time, we adopted the Soumpasis Equation (Soumpasis, 1983) to fit into the measured normalized intensity as a function of time using a mean square error function (Bickel and Doksum, 2015)

$$\overline{I(t)} = e^{-\omega^2/2Dt}\left(B_0\left(\omega^2/2Dt\right) + B_1\left(\omega^2/2Dt\right)\right) \tag{1}$$

where $\overline{I(t)} = [I(t) - I(0)]/[I(\infty) - I(0)]$ is the normalized intensity with $I(t)$ being the measured recovery intensity, $I(0)$ being the intensity immediately after bleaching and $I(\infty)$ being the intensity after recovery. In Eq. (1), ω is the radius of the bleached spot, t is the time, D is the diffusion coefficient, and B_0 and B_1 are the first kind modified Bessel functions of order 0 and 1, respectively. Fig. 2e plots the experimental data and theoretical fitting curve of the recovery intensity as a function of time for extracting FITC diffusivity.

3.3. Experiment results

We used three FITC-dextran particles of different molecular weights in the experiments. The hydrodynamic diameter of FITC-dextran molecule d_s is correlated with its molecular weight. The relationship between the diameter d and the weight-average

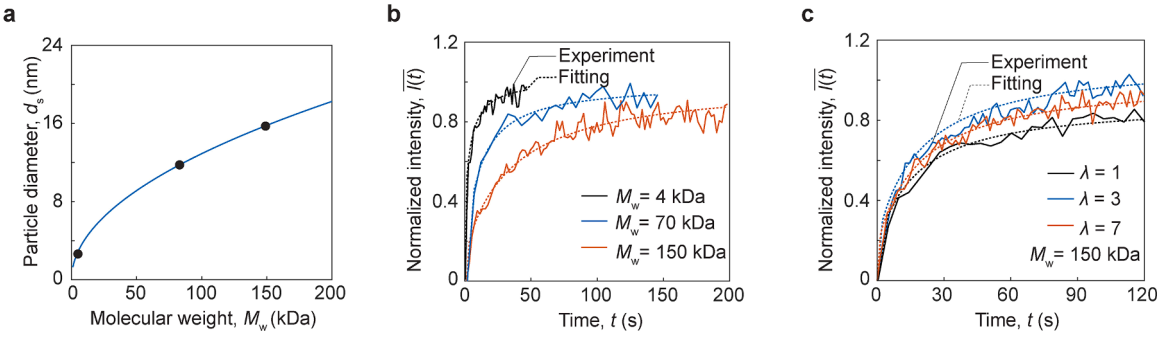


Fig. 3. FRAP characterization of FITC particles with various molecular weights. (a) Hydrodynamic diameter d_s of FITC molecules versus corresponding molecular weight M_w. (b) Normalized intensity versus time for diffusion of FITC with different molecular weights in undeformed hydrogels. (c) Normalized intensity versus time for diffusion of FITC with molecular weight of 150 kDa in hydrogels subjected to various uniaxial stretch ratios.

molecular weight M_w can be estimated using an empirical formula (Amsden, 2022)

$$d_s = 0.408 M_w^{0.5} \tag{2}$$

Following Eq. (2), the diameters of the three types of FITC-dextran (FD) are approximately 2.6 nm, 10.8 nm, and 15.8 nm (Fig. 3a), respectively. Firstly, we conducted the FRAP experiments on undeformed hydrogels mixed with the three FITC particles. The three normalized recovery curves at the undeformed state and their fitting curves are plotted in Fig. 3b. The curve for the small particles (e.g., 4 kDa FITC) shows a rapid recovery with a steep slope within one minute while the curves of large particles (e.g., 70 kDa and 150 kDa FITC) recover more slowly with a flatter slope over three minutes. Applying Eq. (1), the diffusivity of these three particles in the undeformed hydrogels is approximately 1.62×10^{-11} m^2/s, 1.13×10^{-12} m^2/s, and 0.87×10^{-13} m^2/s, respectively. Following the Stokes-Einstein equation, the diffusivity of these three particles in pure water is about 1.68×10^{-10} m^2/s, 4.07×10^{-11} m^2/s, and 2.78×10^{-11} m^2/s. Compared with the diffusivity in pure water, the diffusivity of 4 kDa FITC in polymeric medium decreases to 1/10 that in pure water, while the diffusivity of 70 kDa FITC and 150 kDa FITC decreases to 1/36 and 1/320 that in pure water, respectively. The reason is that the large particles need to overcome the elastic energy barrier of polymer chains to diffuse between confined cages in a polymeric medium, leading to a higher reduction in diffusivity compared with that in a pure liquid medium. We further conducted FRAP experiments on pre-stretched hydrogels embedded with fluorescent molecules with controlled uniaxial stretch ratios ranging from 1 to 7. Fig. 3c plots three normalized recovery curves and their fitting curves of 150 kDa FITC under uniaxial stretch ratios of 1, 3, and 7. The recovery curve at $\lambda = 3$ has a slightly sharper slope than that at $\lambda = 1$ and $\lambda = 7$, indicating a larger diffusivity at $\lambda = 3$ compared to that at the undeformed state and $\lambda = 7$. Using the fitting equation Eq. (1), the diffusivities of the three fluorescent molecules in pre-stretched hydrogels with different uniaxial stretch ratios are summarized in Fig. 4. For small particles (e.g., 4 kDa FITC), the diffusivity exhibits a monotonic decrease from 1.62×10^{-11} m^2/s to 1.23×10^{-11} m^2/s as the stretch ratio increases (Fig. 4a). In contrast, for large particles (e.g., 70 kDa and 150 kDa FITC) the diffusivity first increases and then decreases as the stretch ratio increases, which exhibits a non-monotonic trend. For the large particles with a molecular weight of $M_w = 70$ kDa, the highest diffusivity 1.51×10^{-12} m^2/s occurs at a stretch ratio of $\lambda = 2$, with a diffusivity ratio of about 1.5 compared to the diffusivity at undeformed state (Fig. 4b). For the large particles with a molecular weight of $M_w = 150$ kDa, the highest diffusivity of 1.68×10^{-13} m^2/s occurs at a stretch ratio of $\lambda = 3$, with a diffusivity ratio of about 2.1 compared to the diffusivity at undeformed state (Fig. 4c). In summary, the experimental results reveal an intriguing relationship between the diffusivity, particle sizes, and the uniaxial stretch ratios. The diffusivity for small particles exhibits a monotonic trend, while the diffusivity for large particles exhibits a non-monotonic trend when the hydrogel is subjected to uniaxial tension at various stretch ratios. Notably, the diffusivity enhancement ratio and its corresponding uniaxial stretch ratio vary for large particles of different sizes.

4. Mechano-transport theory

To uncover the mechanism of strain-engineered particle diffusivity in stretchable soft materials, we develop a mechano-transport theory to establish the relationship between macroscopic deformation of soft materials and microscopic diffusion of particles. The mechano-transport theory integrates three models (Fig. 5a): 1) the eight-chain model (Arruda and Boyce, 1993) to relate the bulk deformation of soft materials to the stretch state of individual polymer chains, 2) the ideal chain model (Kuhn and Grün, 1942) to calculate the free energy required to stretch an individual polymer chain to a specified stretch state and 3) the particle diffusion models to quantify the diffusivity of particles across diameters. For particles larger than materials' mesh size, we adopt the hopping diffusion model (Cai et al., 2015) to quantify particle diffusivity, which depends on the energy barrier encountered during particle movement; for particles smaller than materials' mesh size, we adopt the obstruction model (Amsden, 1999) to quantify particle diffusivity, which depends on the probability of the particle encountering neighboring polymer chains. Overall, our mechano-transport theory accounts for the synergistic effects of the geometric transformation of polymer networks and the energy modulation of individual polymer chains, governing the particle diffusion in soft materials subjected to controlled mechanical deformation.

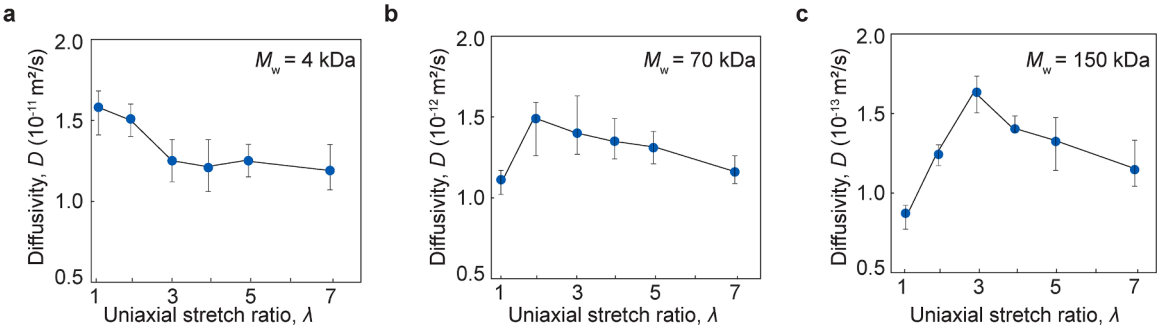


Fig. 4. Measured diffusivity for FITC molecules in hydrogels subjected to uniaxial tension. (a) Diffusivity of 4 kDa FITC versus uniaxial stretch ratio. (b) Diffusivity of 70 kDa FITC versus uniaxial stretch ratio. (c) Diffusivity of 150 kDa FITC versus uniaxial stretch ratio.

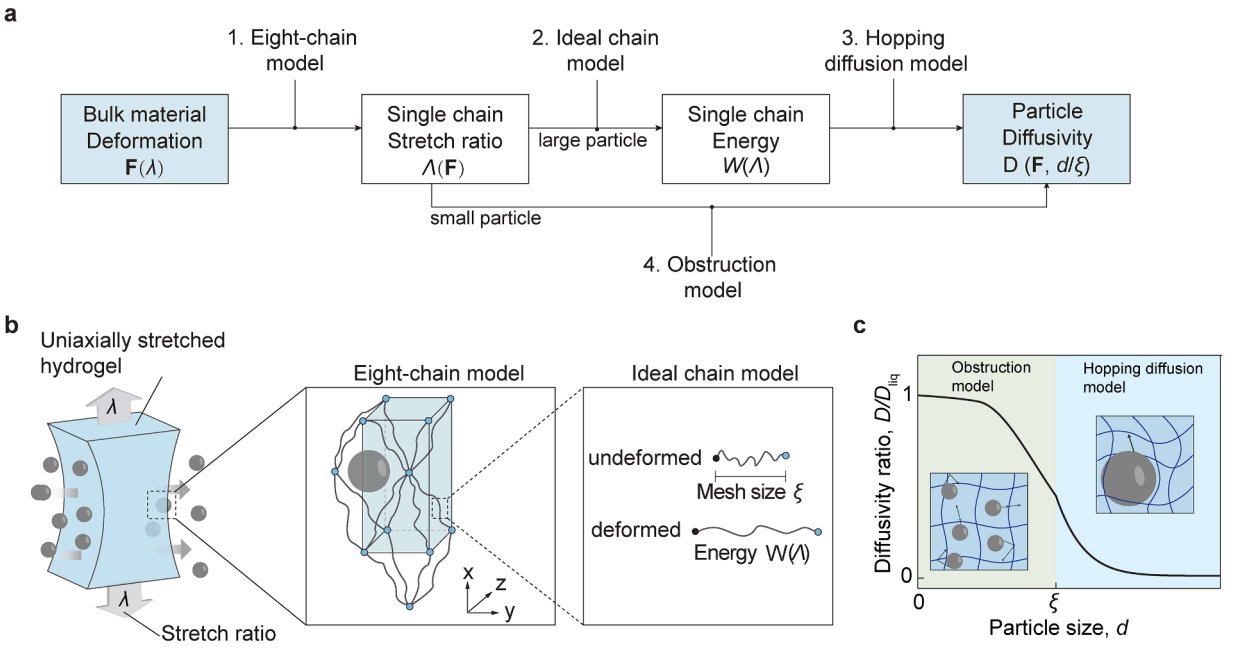


Fig. 5. Mechano-transport theory. (a) Schematic illustration of the mechano-transport theoretical framework that correlates the bulk-material deformation gradient $\mathbf{F}(\lambda)$ with particle diffusivity $D(\mathbf{F},\ d/\xi)$, integrating three models: the eight-chain model to relate single-chain stretch Λ with bulk-material deformation gradient $\mathbf{F}$, the ideal chain model to relate single-chain free energy W with its chain stretch Λ, and the particle diffusion models to relate particle diffusivity D with single chain free energy W. (b) Schematic illustration of the bulk material, the eight-chain model, and the ideal chain model when the bulk material is subjected to uniaxial tension. (c) Illustration of particle diffusivity D in a polymeric gel normalized by liquid diffusivity D_{liq} of its corresponding solvent. If the particle diameter is smaller than the mesh size ($d\ <\ \xi$), particle diffusion is governed by the obstruction model; if the particle diameter is comparable to the mesh size ($d \approx \xi$), particle diffusion is governed by the hopping diffusion model.

4.1. Eight-chain model

The eight-chain model conceptualizes soft materials as a network of eight interconnected chains within a representative cube (Arruda and Boyce, 1993), which approximates the molecular structure of polymeric materials. When the bulk material undergoes mechanical deformation, the eight-chain model accounts for the strain distribution across all chains, thereby capturing the nonlinear elasticity of soft materials. In the eight-chain model, each chain has a chain length $\xi\ =\sqrt{N}b$, where b is the Kuhn length of the polymer chain, and N is the number of statistical segments of Kuhn length between neighboring crosslinkers. When the bulk material is subjected to mechanical deformation, each chain undergoes an equivalent stretch level, following the assumption of affine deformation. The stretch ratio of an individual polymer chain, $\Lambda\ =\xi_{\text{chain}}/\xi$, is correlated with the principal stretches $\lambda_1, \lambda_2, \lambda_3$ imposed on the bulk material, where ξ_{chain} is the polymer chain length after deformation. The stretch ratio of polymer chains is expressed as

$$\Lambda = \sqrt{\frac{1}{3}\left(\lambda_1^2+\lambda_2^2+\lambda_3^2\right)} \tag{3}$$

When an incompressible soft material is subjected to a uniaxial stretch ratio λ, the three principal stretch ratios are $\lambda_1\ =\lambda, \lambda_2 = \lambda_3\ = 1/\sqrt{\lambda}$ (Fig. 5b). Following Eq. (3), the stretch ratio of an individual polymer chain Λ when subjected to uniaxial tension can be expressed as a function of the stretch ratio λ

$$\Lambda = \sqrt{\frac{1}{3}\left(\lambda^2+\frac{2}{\lambda}\right)} \tag{4}$$

From Eq. (4), the stretch ratio of an individual polymer chain Λ increases with the uniaxial stretch ratio λ applied on the bulk materials.

4.2. Ideal chain model

The ideal chain model correlates the free energy of an individual polymer chain with its stretch level (Kuhn and Grün, 1942). The model accounts for the finite extensibility of a polymer chain with its maximum chain length Nb. According to the Langevin statistics, the relationship between an individual polymer chain's force f and its chain length ξ_{chain} is expressed as

$$f = \frac{k_B T}{b}\beta \tag{5}$$

where $\beta = \mathscr{L}^{-1}(\Lambda/\sqrt{N})$ with $\mathscr{L}^{-1}$ being the inverse Langevin function defined by $\mathscr{L}(x) = \coth(x) - 1/x$. By integrating Eq. (5), the free energy of the chain can be expressed as (Zhao, 2012)

$$W = Nk_B T\left(\frac{\beta}{\tanh\beta} + \log\frac{\beta}{\sinh\beta}\right) \tag{6}$$

Given Eq. (6), the energy barrier U of an individual chain subjected to a higher stretch level Λ_H and a lower stretch level Λ_L is expressed as

$$U = W(\Lambda_H) - W(\Lambda_L) \tag{7}$$

As the stretch level increases, the energy barrier of a single polymer chain between its stretched state and its relaxed state rises rapidly. Additionally, a short chain with fewer segments (e.g., $N = 100$) needs to overcome a higher energy barrier compared to a longer chain with more segments (e.g., $N = 2000$) to achieve a same stretch level.

4.3. Particle diffusion model

When particles diffuse in a polymeric medium, the mechanism of particle diffusion is governed by the particle size. Even if the particle size is smaller than the monomer radius, polymer chains can hinder particle diffusion (Fujiyabu et al., 2019). Here, we discuss two particle diffusion models in undeformed hydrogels and categorize them by particle diameter: the obstruction model for particles smaller than the mesh size ($d < \xi$) and the hopping diffusion model for particles comparable to the mesh size ($d \approx \xi$).

When the particle diameter is smaller than the mesh size ($d < \xi$), the movement of particles is restricted by encountering a series of polymer chains that act as obstacles, leading to a reduction in particle diffusivity. The obstruction model (Amsden, 1999) considers polymer chains as randomly oriented straight fibers that hinder the diffusion of small particles (Ogston, 1958). It uses the probability of particles encountering obstacles to express the particle diffusivity in a polymeric gel D normalized by the liquid diffusivity of its corresponding solvent D_{liq}, as follows

$$\frac{D}{D_{liq}} = \exp\left[-\frac{\pi}{4}\left(\frac{d}{\xi}\right)^2\right] \tag{8}$$

According to Eq. (8), the diffusivity decreases by an order of magnitude as the particle size approaches the mesh size.

If the particle diameter is compared to the mesh size ($d \approx \xi$), the movement of particle is temporarily restricted by the confined cages of polymer chains. In this scenario, the particle must overcome an energy barrier to transit from its initial cage to its final cage (Fig. 1b). Following the hopping diffusion model (Cai et al., 2015), the particle diffusivity in an undeformed polymer network can be approximated as

$$D \cong \frac{\xi_c^2}{\tau_r}\left(\frac{d}{\xi}\right)^{-1}\exp\left(-\left(\frac{d}{\xi}\right)^2\right) \tag{9}$$

where ξ_c is the correlation length, and τ_r is the relaxation time of the polymer network. To complete a single hopping step, the particle needs to overcome an energy barrier U, approximately expressed as:

$$\frac{U}{k_B T} \cong \left(\frac{d}{\xi}\right)^2 \tag{10}$$

Combining Eqs. (9) and (10), we can approximate the particle diffusivity D as

$$D \cong \frac{\xi_c^2}{\tau_r}\left(\sqrt{\frac{U}{k_B T}}\right)^{-1}\exp\left(-\frac{U}{k_B T}\right) \tag{11}$$

If particles diffuse in the same material system while overcoming two energy barriers U_1 and U_2, the ratio of particle diffusivities D_1 and D_2 corresponding to the two energy barriers can be expressed as a function of energy barriers U_1 and U_2, writing as

$$\frac{D_1}{D_2} = \sqrt{\frac{U_2}{U_1}}\exp\left(\frac{U_2 - U_1}{k_B T}\right) \tag{12}$$

5. Strain-engineered particle diffusion under uniaxial tension

In this section, we apply the mechano-transport theory to study a specific case: particle diffusion in an incompressible soft material subjected to a controlled uniaxial tensile load. We focus on two cases: 1) the particle diameter is smaller than the polymer mesh size ($d < \xi$), and 2) the particle diameter is comparable to polymer mesh size ($d \approx \xi$).

5.1. Small particles $d < \xi$

For particles smaller than the polymer mesh size, the particle diffusion is restricted by polymer chains and governed by the obstruction model. From Eq. (8), the diffusion process is correlated with the mesh size ξ of the polymer network. When the hydrogel is subject to uniaxial tension with a stretch ratio λ (e.g., along x-axis), the three principal stretch ratios are $\lambda_1 = \lambda$, $\lambda_2 = \lambda_3 = 1/\sqrt{\lambda}$. The two-dimensional square cage perpendicular to the stretch direction (e.g., x-axis) contracts uniformly with a ratio $\lambda_x = 1/\sqrt{\lambda}$ (Fig. 6b). The mesh size along the stretch direction becomes $\xi_x = \xi/\sqrt{\lambda}$. Meanwhile, the shape in the direction perpendicular to the stretch direction (e.g., y-axis) deforms into a rhombus cage with a ratio along the long axis $\lambda_l = \lambda$ and a ratio along the short axis $\lambda_s = 1/\sqrt{\lambda}$ (Fig. 7b). We consider the length along the short axis as the effective mesh size, which contracts with a ratio λ_s, giving an effective mesh size of $\xi_s = \xi/\sqrt{\lambda}$. Applying Eq. (8), the particle diffusivity ratio D/D_0 is expressed as

$$\frac{D}{D_0} = \exp\left[-\frac{\pi}{4}\frac{(\lambda-1)d^2}{\xi^2}\right] \tag{13}$$

where D is the particle diffusivity at deformed state and D_0 is the particle diffusivity at undeformed state. As shown in Fig. 6c, the diffusivity exhibits a monotonic decrease as the uniaxial stretch ratio increases. The reduction of D is more pronounced for larger particles (e.g., $d/\xi = 0.5$) than smaller particles (e.g., $d/\xi = 0.1$). For larger particles (e.g., $d/\xi = 0.5$), the deformation of polymer chains significantly impacts the diffusion process. Following the mechano-transport theory based on the obstruction model, the particle diffusivity solely depends on the geometric transformation of the polymer network and exhibits the same diffusivity along different axes (e.g., along x-axis and y-axis). For even larger particles that are comparable to the mesh size, both the elastic energy of polymer chains and the geometric deformation of the polymer network should be considered in the diffusion process, which will be discussed in the following section.

5.2. Large particles $d \approx \xi$

For particles comparable to the polymer mesh size, the particles need to overcome an energy barrier to transit from one confined cage to an adjacent one, following the hopping diffusion model. To compare with the diffusivity in the hydrogel at undeformed state, in this section, we first calculate the energy barrier needed for particles to diffuse in an undeformed hydrogel. Next, to determine the energy barrier experienced by particles diffusing along different axes, we further quantify the synergistic contributions from the

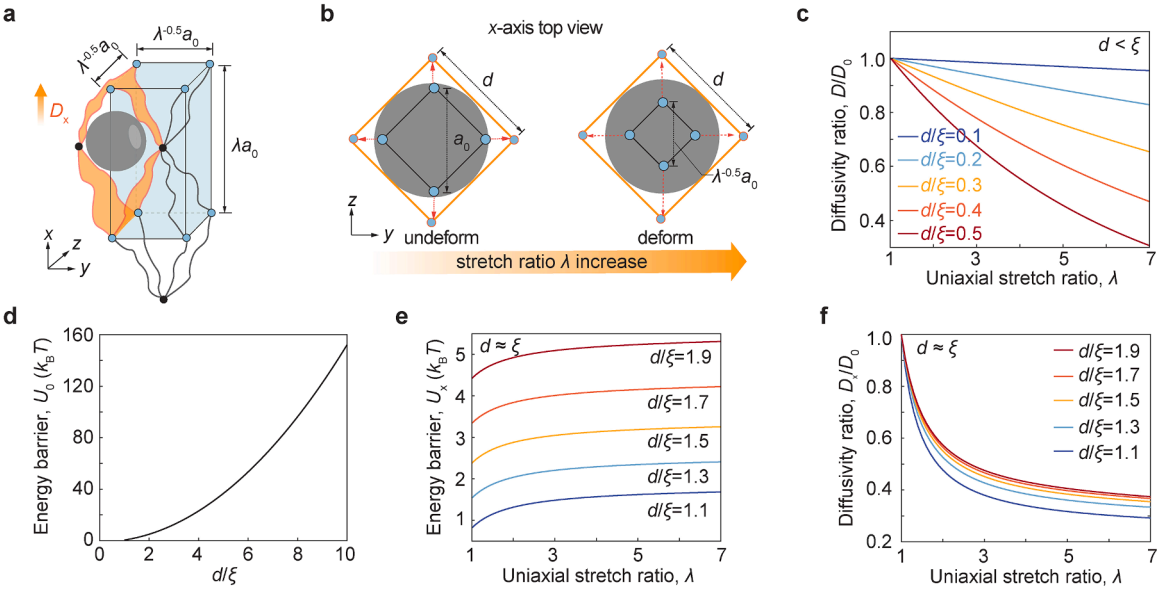


Fig. 6. Particle diffusion parallel to the stretch direction under uniaxial tension. (a) Schematic illustration of particle diffusion along the stretch direction (x-axis). (b) Top view schematics from the x-axis at the undeformed and deformed states. The black lines depict the confined cage without particles projected to the yz plane at the undeformed and deformed states and the orange lines depict the corresponding cage that allows particles to pass through. The orange dashed arrow indicates the stretched directions. (c) Particle diffusivity ratio D/D_0 between the deformed state and undeformed state as a function of uniaxial stretch ratio λ for particles with varying diameters d smaller than the mesh size ξ. (d) Energy barrier U experienced by particles in the undeformed polymer network is a function of the ratio between particle diameter d and mesh size. (e) Energy barrier experienced by particles U as a function of uniaxial stretch ratio λ for particles with varying diameters d slightly larger than the mesh size ξ. (f) Particle diffusivity ratio parallel to the stretch direction (e.g., x-axis). D_x/D_0 between the deformed state and undeformed state as a function of uniaxial stretch ratio λ for particles with varying diameters slightly larger than the mesh size.

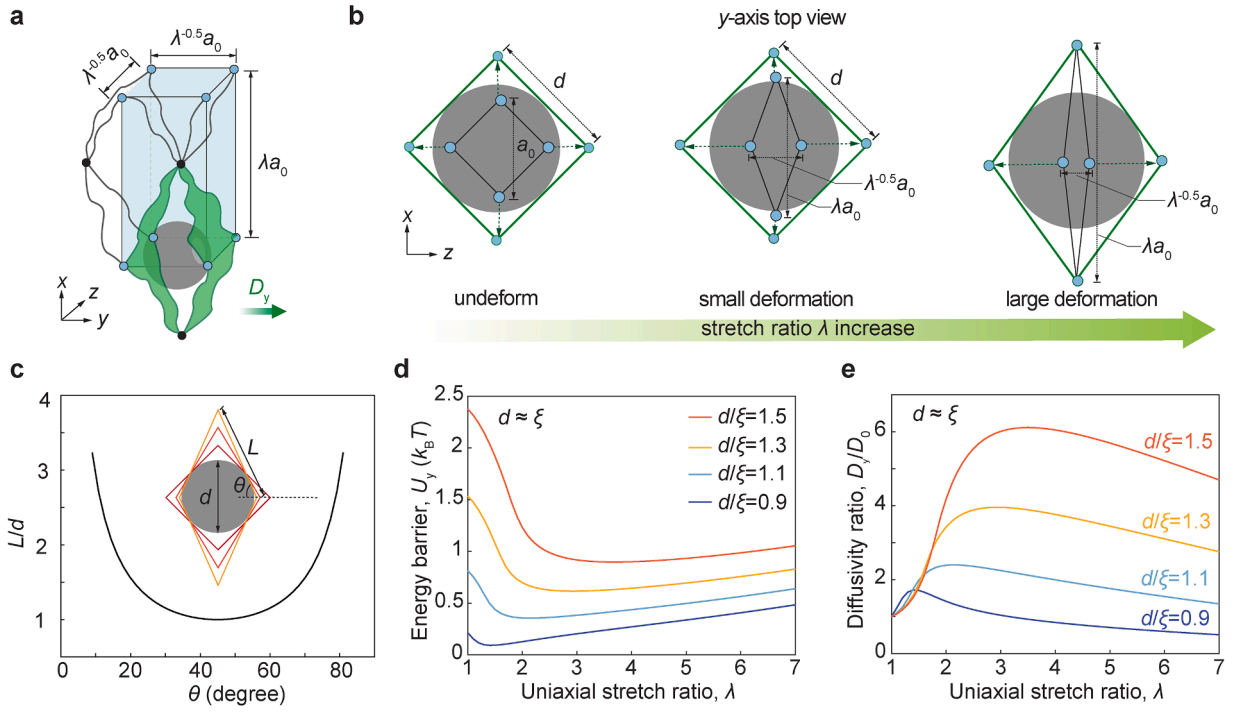


Fig. 7. Particle diffusion perpendicular to the stretch direction under uniaxial tension. (a) Schematic illustration of particle diffusion perpendicular to the stretch direction (*y*-axis). (b) Top view schematics of the *y*-axis as the stretch ratio increases. The black lines depict the confined cage at undeformed, small and large deformed states, while the green lines depict the cage that allows particles to pass through. The green dashed arrow indicates the stretched directions. (c) Side length of the rhombus L normalized by the particle diameter d as a function of the angle θ. The schematic illustrates the geometrical configuration of the rhombus with its sides tangential to the circumference of the particle. (d) Energy barrier experienced by particles U as a function of uniaxial stretch ratio λ for particles with varying diameters d slightly larger than the mesh size ξ. (e) Particle diffusivity ratio perpendicular to the stretch direction (e.g., *y*-axis) D_y/D_0 between the deformed state and undeformed state as a function of uniaxial stretch ratio λ for particles with varying diameters slightly larger than the mesh size.

geometric transformation of polymer network and the energy modulation of polymer chains.

5.2.1. *Particle diffusion at undeformed state*

According to Eq. (7), particle diffusivity is determined by the lower limit ξ_L and the higher limit ξ_H of chain length associated with particle diffusion. At undeformed state, the lower limit chain length is equal to its initial chain length ($\xi_L = \xi$), giving the chain stretch ratio $\Lambda_L = 1$. To identify the higher limit chain length ξ_H, we consider the two-dimensional cage encapsulating the particle, normal to the *x*-axis. As illustrated in Fig. 6b, the black square cage, which depicts the polymer network shape at undeformed state, needs to be stretched to the orange square cage to allow the particle to pass through. The four side lengths of the cage are stretched uniformly until the circumference of the particle is tangential to the cage, allowing the particle to pass through. To calculate the higher limit chain length (Fig. 6b), the side length of the cage needs to reach the diameter of the particle d. Therefore, the chain length is $\xi_H = \sqrt{d^2 + a_0{}^2/4}$, where $a_0 = 2/\sqrt{3}\xi$ is the edge length of the cube. The corresponding stretch ratio of the polymer chain length $\Lambda_H = \xi_H/\xi$ is expressed as

$$\Lambda_H = \sqrt{\left(\frac{d}{\xi}\right)^2 + \frac{1}{3}} \tag{14}$$

Following Eq. (7), the energy barrier needed for the particle to hop between neighboring cages in an undeformed soft material is expressed as

$$U_0 = W\left(\sqrt{\left(\frac{d}{\xi}\right)^2 + \frac{1}{3}}\right) - W(1) \tag{15}$$

where U_0 is the energy barrier for particles to diffuse in an undeformed soft material. In Eq. (15), the energy barrier U_0 is a function of the ratio between the particle diameter and the mesh size d/ξ. The curve in Fig. 6d shows that energy barrier increases drastically with d/ξ, which indicates the polymer needs overcome a higher energy barrier to allow larger particles to pass through.

5.2.2. Particle diffusion parallel to the stretch direction at deformed state

Following the discussion in Section 5.1, the square cage normal to the *x*-axis, as depicted by the black line in Fig. 6b, contracts with a ratio $1/\sqrt{\lambda}$ when the bulk material is subjected to uniaxial tension. Similar to the undeformed state, the length of the 2D square cage needs to reach the particle diameter of the particle d to allow the particle to pass through along the *x*-axis (Fig. 6b). The higher limit chain length reaches $\xi_{\mathrm{H}}^{x} = \left(d^2 + \lambda^2 a_0^2/4\right)^{1/2}$. The stretch ratio of the higher limit chain length $\Lambda_{\mathrm{H}}^{x} = \xi_{\mathrm{H}}^{x}/\xi$ is expressed as

$$\Lambda_{\mathrm{H}}^{x} = \sqrt{\left(\frac{d}{\xi}\right)^2 + \frac{1}{3}\lambda^2} \tag{16}$$

Compared to the undeformed state, the polymer chain undergoes a stretch ratio of Λ (Eq. (4)) when subjected to uniaxial tension. The stretch ratio of the lower limit chain length is $\Lambda_{\mathrm{L}}^{x} = \Lambda$. Following the Eq. (7), the energy barrier needed for the particle to diffuse through polymer network parallel to the stretch direction (e.g., *x*-axis) is $U_x = W\left(\Lambda_{\mathrm{H}}^{x}\right) - W\left(\Lambda_{\mathrm{L}}^{x}\right)$. Combined with Eq. (16), the energy barrier U_x is expressed as

$$U_{\mathrm{x}} = W\left(\sqrt{\left(\frac{d}{\xi}\right)^2 + \frac{1}{3}\lambda^2}\right) - W\left(\sqrt{\frac{1}{3}\left(\lambda^2 + \frac{2}{\lambda}\right)}\right) \tag{17}$$

Compared to U_0 in Eq. (15), the energy barrier U_x is a function of two parameters: the ratio between particle size and mesh size d/ξ and the applied stretch ratio λ. These two parameters synergistically determine both the stretch state of the polymer chain and the geometric deformation of polymer networks. Furthermore, the value of energy barrier is also correlated with the function of free energy W, which is determined by the ideal chain model in our theory. For instance, when particles diffuse through biological tissues, the worm-like chain model (Rubinstein and Colby, 2003) is suitable for describing the semi-flexible polymer networks. The energy W required to reach the same high stretch state will be significantly increased, resulting in a larger difference in particle diffusivity between the deformed state and the undeformed state.

We quantitively study the energy barriers for particles with various diameters under different stretch levels. Fig. 6e shows that as the stretch ratio increases, the energy barrier rises unitil it reaches a plateau. Following this, we employ Eq. (12) to calculate the diffusivity at deformed state along the *x*-axis relative to that at undeformed state D_x/D_0, which is expressed as

$$\frac{D_x}{D_0} = \sqrt{\frac{U_0}{U_x}}\exp\left(\frac{U_0 - U_x}{k_{\mathrm{B}}T}\right) \tag{18}$$

As shown in Fig. 6f, the diffusivity ratio is a function of the uniaxial stretch ratio λ for particles with varying diameters slightly larger than the mesh size. Similar to the energy barrier U_x, we observe the ratio D_x/D_0 increases with the stretch ratio until it plateaus.

5.2.3. Particle diffusion perpendicular to the stretch direction at the deformed state

When a hydrogel is subjected to uniaxial tension, the square cage normal to the *y* and *z* axis evolves to a rhombus with a long axis $l_{\mathrm{l}} = \lambda a_0$ and a short axis $l_{\mathrm{s}} = 1/\sqrt{\lambda} a_0$. The black cage in Fig. 7b illustrates the square cages normal to the unstretched direction at the undeformed state, gradually deforming into the rhombus cage at small and large deformed states as the uniaxial stretch ratio increases. To enable particles to pass through, the rhombus cage can deform into various shapes, each corresponding to a distinct energy barrier. We use the lowest energy barrier among these possibilities to determine the diffusion along the *y* and *z* axes. Identifying the lowest energy barrier is equivalent to identifying a stretched rhombus with the minimum side length whose boundary is tangential to the circumference of the particle. All the rhombi with various shapes that are tangential to the particle are drawn in Fig. 7c. The side length L of the rhombus can be quantified by the angel θ, which determines the shape of each rhombus, as $L = \tan(\theta)\cdot d/2 + d/(2\cdot\tan(\theta))$. We plot the side length L as a function of θ in Fig. 7c, which shows a minimum value of L at $\theta = 45^o$. As the stretch ratio increases, the length of the long axis becomes longer while the length of short axis becomes shorter. Due to the differing minimum energy barrier associated with the geometric transformation, we separate the diffusion analysis perpendicular to the stretch direction (e.g., *y*-axis) into two cases: the length of the long axis l_{l} shorter than the diagonal length of the square tangential to the particle with diameter d ($l_{\mathrm{l}} < \sqrt{2}d$), and the length of the long axis l_{l} longer than the diagonal length of the square tangential to the particle with diameter d ($l_{\mathrm{l}} > \sqrt{2}d$).

As depicted in Fig. 7a, from a three-dimension view, the higher limit chain length is equal to

$$\xi_{\mathrm{H}}^{y} = \sqrt{L_{xz}^2 + L_y^2} \tag{19}$$

where L_{xz} is the length of rhombus cage length in the *xz* plane (Fig. 7b), and $L_y = 0.5\lambda^{-0.5}a_0$ is the half length of the deformed cuboid in the *xz* plane. When the stretch ratio is low, as illustrated by the black cage at small deformation in Fig. 7b, the rhombus shape remains inside the particle shape, where $l_{\mathrm{l}} < \sqrt{2}d$. To ensure the particle can pass through the confinement cage with the minimum energy barrier, the rhombus cage needs to be stretched to a square cage with side length equal to $L_{xz} = d$, whose angle is $\theta = 45^o$ as shown in Fig. 7c. Substituting the lengths of L_y and L_{xz} back to Eq. (19), the higher limit chain length is expressed as

$$\xi_{\mathrm{H}}^{y} = \left(d^2 + a_0^2/4\lambda\right)^{1/2} \quad \text{for} \quad l_{\mathrm{l}} < \sqrt{2}d \tag{20}$$

When the stretch ratio is higher, as illustrated by the black cage at large deformation in Fig. 7b, the long axis of the rhombus shape exceeds the particle shape, where $l_l > \sqrt{2}d$. To avoid the stretched rhombus achieving an even larger θ, as depicted by the green cage at large deformation in Fig. 7b, we keep the length of the long axis l_l unchanged while stretching the length of the short axis l_s until the boundary of the cage is tangential to the shape of the particle. As a result, the length of rhombus cage L_{xz} is expressed as

$$L_{xz} = \frac{\lambda a_0}{2\cos\left(\arcsin\left(\frac{d}{\lambda a_0}\right)\right)} \tag{21}$$

Substituting the lengths of L_y and L_{xz} back to Eq. (19), the higher limit chain length is expressed as

$$\xi^y_{\mathrm{H}} = \frac{a_0}{2}\sqrt{\lambda^2\left(1+\tan^2\left(\arcsin\left(\frac{d}{\lambda a_0}\right)\right)\right)+\frac{1}{\lambda}} \quad \text{for} \quad l_l > \sqrt{2}d \tag{22}$$

In summary, the stretch ratio of high limit chain length for the two cases is expressed as

$$\Lambda^y_{\mathrm{H}} = \begin{cases} \sqrt{\left(\frac{d}{\xi}\right)^2+\frac{1}{3\lambda}}, & \text{for } l_l < \sqrt{2}d \\ \sqrt{\frac{1}{3}\lambda^2\left(1+\tan^2\left(\arcsin\left(\frac{\sqrt{3}}{2\lambda}\left(\frac{d}{\xi}\right)\right)\right)\right)+\frac{1}{3\lambda}}, & \text{for } l_l > \sqrt{2}d \end{cases} \tag{23}$$

Similar to the diffusion parallel to the stretch direction, the polymer chain undergoes a stretch ratio of Λ due to bulk deformation without the presence of the particle, which defines the lower limit chain stretch ratio, namely $\Lambda^y_{\mathrm{L}} = \Lambda = \sqrt{\frac{1}{3}\left(\lambda^2+\frac{2}{\lambda}\right)}$. The energy barrier needed for the particle to diffuse perpendicular to the stretch direction (e.g., y-axis) when subjected to uniaxial tension is expressed as

$$U_y = W(\Lambda^y_{\mathrm{H}}) - W(\Lambda^y_{\mathrm{L}}) \tag{24}$$

According to Eq. (24), the energy barrier U_y is a function of d/ξ and λ. We quantitively investigate the energy barriers for particles of various diameters under different levels of stretch. In Fig. 7d, the energy barrier displays a non-monotonic trend as the stretch ratio increases. Although the polymer chains have the same stretch state when the bulk material is subjected to uniaxial tension, the energy barrier along the x-axis shows a monotonic increasing trend, while the energy barrier along the y-axis shows a non-monotonic trend. This is because the mechanical deformation results in a different geometries in the polymer network along various directions. This difference results in variations in the energy barrier variation and consequently a diffusivity difference along different directions, which is anisotropic compared to isotropic behavior at undeformed state. Then we employ Eq. (12) to compare the diffusivity of the deformed state along the y-axis with respect to the undeformed state, which is expressed as

$$\frac{D_y}{D_0} = \sqrt{\frac{U_0}{U_y}}\exp\left(\frac{U_0-U_y}{k_{\mathrm{B}}T}\right) \tag{25}$$

As shown in Fig. 7e, the ratio D_y/D_0 also shows a non-monotonic trend, increasing to a maximum value and then decreasing as the stretch ratio increases. The maximum enhancement and the stretch ratio at which the peak value occurs are both correlated with the particle diameter. As the particle diameter increases, both the maximum enhancement and its corresponding stretch ratio increase.

6. Results and discussion

6.1. Theoretical results

The mesh size of the PAAm-hydrogel is estimated as $\xi = 11.6$ nm, using $\xi = \sqrt{N}b$, where N is the ratio of monomer density to crosslinker density and $b = 0.3$ nm is the Kuhn length of the AAm monomer (Li et al., 2014). Given the identified hydrodynamic diameter of FITC molecules, the ratio between the diameters of three FITC molecules and the mesh size of PAAm-hydrogel is estimated approximately 0.22, 0.93, and 1.36, respectively.

To align with the FRAP measurement which measures the average diffusivity in the horizontal plane (e.g., xy plane), we calculate the theoretical diffusivity by averaging the diffusivity along the x and y axis as $D = (D_x + D_y)/2$, where D is the average diffusivity in the horizontal plane, and D_x and D_y are the diffusivities along the x and y axes, respectively. For the 4 kDa FITC particle ($d/\xi = 0.22$), whose size is smaller than the mesh size, we use the obstruction model with Eq. (13) to calculate the diffusivity. In contrast, for the 70 kDa and 150 kDa FITC particles ($d/\xi = 0.93, 1.36$), whose sizes are comparable to the mesh size, we apply Eqs. (18, 25) to calculate the diffusivity by accounting for the energy barrier needed for particles to leave the confinement cage.

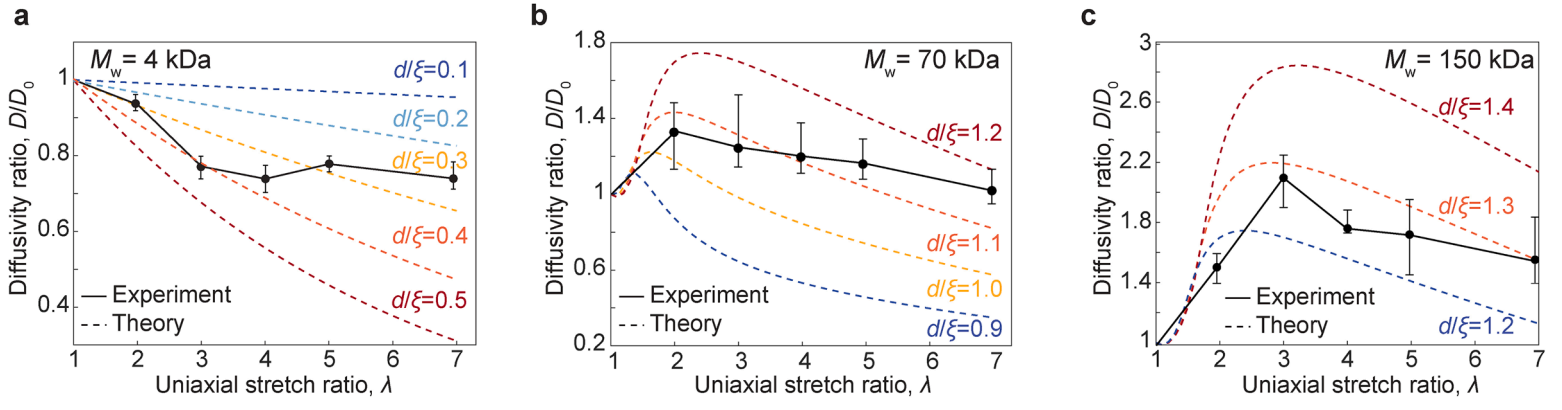


Fig. 8. Comparison between experimental and theoretical results. (a) Plot of the diffusivity ratio between experimental results of FITC particles with $M_w = 4$ kDa and theoretical results for particles with $d/\xi = 0.1 \sim 0.5$. (b) Plot of the diffusivity ratio between experimental results of FITC particles with $M_w = 70$ kDa and theoretical results for particles with $d/\xi = 0.9 \sim 1.2$. (c) Plot of the diffusivity ratio between experimental results of FITC particles with $M_w = 150$ kDa and theoretical results for particles with $d/\xi = 1.2 \sim 1.4$.

6.2. Comparison between experimental and theoretical results

To compare the experimental and theoretical results, as shown in Fig. 8, we plot the experimental diffusivity ratio at deformed state to its undeformed state for each FITC particle, along with the theoretical results, over a wide range of ratios between the particle diameter and the hydrogel mesh size. Fig. 8a shows the experimental results of 4 kDa FITC particle ($d/\xi = 0.22$), and the theoretical plots of particle diameter to mesh size ranging from 0.1 to 0.5. The diffusivity ratio of 4 kDa FITC gradually decrease from 1 to 0.8 as stretch ratio increases from 1 to 7, which shows a good agreement with the theoretical curves of $d/\xi = 0.2\sim0.3$. This indicates that small particles exhibit a monotonic decreasing trend in diffusivity when subjected to uniaxial tension. Fig. 8b and c show the experimental results of 70 kDa FITC ($d/\xi = 0.93$) and 150 kDa FITC ($d/\xi = 1.36$), respectively, along with the theocratical curves. In Fig. 8b, the diffusivity ratio of 70 kDa FITC initially increases to a maximum value about 1.35 at $\lambda = 2$, followed by a decrease as the stretch ratio increases. Similarly, the diffusivity ratio of 150 kDa FITC increases to a maximum ratio about 2.1 at $\lambda = 3$ and then decreases as the stretch ratio increases in Fig. 8c. When compared with the theoretical results, both the 70 kDa and 150 kDa FITC particles exhibit a non-monotonic trend with the increase of the stretch ratio. The 70 kDa FITC shows good agreement with the theoretical curves for $d/\xi = 1.1\sim1.2$, while it has a slight difference with the theoretical curves $d/\xi = 0.9\sim1.0$. The underlying reason is that when the particle size is comparable to the polymer mesh size, the particle can either directly pass through the polymer network without deforming the polymer chains or hop through the polymer network by slightly deforming the polymer chains. The 150 kDa FITC, as shown in Fig. 8c, shows good agreement with the theoretical curves for $d/\xi = 1.3$. This correspondence suggests that the mechano-transport theory offers a framework for predicting particle diffusion in stretchable polymeric medium.

7. Conclusion

In conclusion, our study presents a comprehensive analysis of particle diffusion in a polymeric medium subjected to uniaxial tension. To evaluate particle diffusivity in deformed hydrogels, we conduct FRAP experiments on pre-stretched hydrogels embedded with fluorescent particles of varying sizes. The experimental results reveal an intriguing transition in the relationship between particle diffusivity and uniaxial stretch ratios, characterized by a monotonic decrease for small particles and a non-monotonic trend for large particles. To explain these findings, we integrate three models to formulate a mechano-transport theory. The theory enables a fundamental understanding of how changes at the larger scale of bulk material deformation impact the movement and behavior of particles on a much smaller scale. Through theoretical and experimental analysis, we find that the diffusivity is governed by two dimensionless parameters: the ratio of particle diameter to mesh size, and the ratio of current polymer chain length to its initial length. The diffusivity changes for particles whose diameters are comparable to the mesh size in our experimental data align well with our theoretical predictions, affirming the validity of the mechano-transport theory. It should be noted that in addition to the elasticity of the network, the inherent characteristics (i.e., viscosity and temperature) of the solvent and the interactions between the functionalized hydrogel and particles impact the particle diffusion process. For example, if the functional groups within the hydrogel form covalent bonds with target particles, the particles are arrested inside the polymer network; in contrast, if the functional groups form reversible interactions with target particles, this leads to walking diffusion across the hydrogels (Gu et al., 2021; Yang et al., 2018). Future work will aim to better understand particle diffusion in stretchable polymeric mediums, particularly under complex mechanical loading. Additionally, we will explore the impact of bonding dynamics in the interactions between particles and hydrogel, further investigating how these interactions affect particle behavior in the polymeric medium.

CRediT authorship contribution statement

Jiabin Liu: Conceptualization, Methodology, Formal analysis, Investigation, Writing – original draft, Writing – review & editing. **Shaoting Lin:** Conceptualization, Methodology, Investigation, Writing – original draft, Writing – review & editing, Supervision, Funding acquisition.

Declaration of competing interest

The authors declare the following financial interests/personal relationships which may be considered as potential competing interests: Shaoting Lin reports financial support was provided by Michigan State University. Shaoting Lin reports financial support was provided by National Science Foundation. If there are other authors, they declare that they have no known competing financial interests or personal relationships that could have appeared to influence the work reported in this paper.

Acknowledgements

We thank Dr. Melinda Frame at the Center for Advanced Microscopy for help with the confocal microscopy experiment. We acknowledge the funding support from the National Science Foundation (CBET-2320716). We acknowledge the startup funds from the College of Engineering at Michigan State University.

References

Ahmed, E.M., 2015. Hydrogel: preparation, characterization, and applications: a review. J. Adv. Res. 6, 105–121.

Amsden, B., 1999. An obstruction-scaling model for diffusion in homogeneous hydrogels. Macromolecules 32, 874–879.
Amsden, B.G., 2022. hydrogel mesh size and its impact on predictions of mathematical models of the solute diffusion coefficient. Macromolecules 55, 8399–8408.
Anselmo, A.C., Mitragotri, S., 2017. Impact of particle elasticity on particle-based drug delivery systems. Adv. Drug Deliv. Rev. 108, 51–67.
Arruda, E.M., Boyce, M.C., 1993. A three-dimensional constitutive model for the large stretch behavior of rubber elastic materials. J. Mech. Phys. Solids. 41, 389–412.
Bickel, P.J., Doksum, K.A., 2015. Mathematical Statistics: Basic Ideas and Selected Topics. CRC Press. Volumes I-II Package.
Bouklas, N., Huang, R., 2012. Swelling kinetics of polymer gels: comparison of linear and nonlinear theories. Soft Matter 8, 8194–8203.
Cai, L.H., Panyukov, S., Rubinstein, M., 2015. Hopping diffusion of nanoparticles in polymer matrices. Macromolecules 48, 847–862.
Einstein, A., 1905. On the motion of small particles suspended in liquids at rest required by the molecular-kinetic theory of heat. Ann. Phys. 17, 208.
Fujiyabu, T., Li, X., Chung, U.i., Sakai, T., 2019. Diffusion behavior of water molecules in hydrogels with controlled network structure. Macromolecules 52, 1923–1929.
Gu, Y., Distler, M.E., Cheng, H.F., Huang, C., Mirkin, C.A., 2021. A general DNA-gated hydrogel strategy for selective transport of chemical and biological cargos. J. Am. Chem. Soc. 143, 17200–17208.
Huebsch, N., Kearney, C.J., Zhao, X., Kim, J., Cezar, C.A., Suo, Z., Mooney, D.J., 2014. Ultrasound-triggered disruption and self-healing of reversibly cross-linked hydrogels for drug delivery and enhanced chemotherapy. Proc. Natl. Acad. Sci. 111, 9762–9767.
Kim, T., Song, W., Son, D.Y., Ono, L.K., Qi, Y., 2019. Lithium-ion batteries: outlook on present, future, and hybridized technologies. J. Mater. Chem. A 7, 2942–2964.
Kuhn, W., Grün, F., 1942. Beziehungen zwischen elastischen Konstanten und Dehnungsdoppelbrechung hochelastischer Stoffe. Kolloid-Zeitschrift 101, 248–271.
Li, A., Ramakrishna, S.N., Nalam, P.C., Benetti, E.M., Spencer, N.D., 2014. Stratified polymer grafts: synthesis and characterization of layered 'brush'and 'gel'structures. Adv. Mater. Interfaces 1, 1300007.
Li, J., Mooney, D.J., 2016. Designing hydrogels for controlled drug delivery. Nat. Rev. Mater. 1, 1–17.
Lin, S., Wang, B., Zhao, Y., Shih, R., Cheng, X., Yu, W., Hojaiji, H., Lin, H., Hoffman, C., Ly, D., 2019. Natural perspiration sampling and *in situ* electrochemical analysis with hydrogel micropatches for user-identifiable and wireless chemo/biosensing. ACS Sens. 5, 93–102.
Lin, S., Yuk, H., Zhang, T., Parada, G.A., Koo, H., Yu, C., Zhao, X., 2016. Stretchable hydrogel electronics and devices. Adv. Mater. 28, 4497–4505.
Liu, J., Yang, C., Yin, T., Wang, Z., Qu, S., Suo, Z., 2019. Polyacrylamide hydrogels. II. Elastic dissipater. J. Mech. Phys. Solids 133, 103737.
Long, R., Hui, C.Y., 2016. Fracture toughness of hydrogels: measurement and interpretation. Soft Matter 12, 8069–8086.
Lorén, N., Hagman, J., Jonasson, J.K., Deschout, H., Bernin, D., Cella-Zanacchi, F., Diaspro, A., McNally, J.G., Ameloot, M., Smisdom, N., 2015. Fluorescence recovery after photobleaching in material and life sciences: putting theory into practice. Q. Rev. Biophys. 48, 323–387.
Ogston, A., 1958. The spaces in a uniform random suspension of fibres. Trans. Faraday Soc. 54, 1754–1757.
Poling, B.E., Prausnitz, J.M., O'Connell, J.P., 2001. The Properties of Gases and Liquids, 5th Edition. https://doi.org/10.1036/0070116822.
Raju, S., Carbery, M., Kuttykattil, A., Senthirajah, K., Lundmark, A., Rogers, Z., Suresh, S., Evans, G., Palanisami, T., 2020. Improved methodology to determine the fate and transport of microplastics in a secondary wastewater treatment plant. Water Res. 173, 115549.
Rubinstein, M., Colby, R.H., 2003. Polymer Physics. Oxford university press.
Schwartz, G., Morejon, A., Best, T.M., Jackson, A.R., Travascio, F., 2022. Strain-dependent diffusivity of small and large molecules in meniscus. J. Biomech. Eng. 144, 111010.
Soumpasis, D., 1983. Theoretical analysis of fluorescence photobleaching recovery experiments. Biophys. J. 41, 95–97.
Sun, W., Jiang, H., Wu, X., Xu, Z., Yao, C., Wang, J., Qin, M., Jiang, Q., Wang, W., Shi, D., 2019. Strong dual-crosslinked hydrogels for ultrasound-triggered drug delivery. Nano Res. 12, 115–119.
Wang, J., Kaplan, J.A., Colson, Y.L., Grinstaff, M.W., 2017. Mechanoresponsive materials for drug delivery: harnessing forces for controlled release. Adv. Drug Deliv. Rev. 108, 68–82.
Xiang, Y., Zhong, D., Wang, P., Mao, G., Yu, H., Qu, S., 2018. A general constitutive model of soft elastomers. J. Mech. Phys. Solids 117, 110–122.
Yang, Y.J., Mai, D.J., Dursch, T.J., Olsen, B.D., 2018. Nucleopore-inspired polymer hydrogels for selective biomolecular transport. Biomacromolecules 19, 3905–3916.
Yang, C., Yin, T., Suo, Z., 2019. Polyacrylamide hydrogels. I. Network imperfection. J. Mech. Phys. Solids 131, 43–55.
Zhang, S., Zeng, M., Li, J., Li, J., Xu, J., Wang, X., 2014. Porous magnetic carbon sheets from biomass as an adsorbent for the fast removal of organic pollutants from aqueous solution. J. Mater. Chem. A 2, 4391–4397.
Zhang, Y., Yu, J., Bomba, H.N., Zhu, Y., Gu, Z., 2016. Mechanical force-triggered drug delivery. Chem. Rev. 116, 12536–12563.
Zhao, X., 2012. A theory for large deformation and damage of interpenetrating polymer networks. J. Mech. Phys. Solids 60, 319–332.
Zhao, X., Kim, J., Cezar, C.A., Huebsch, N., Lee, K., Bouhadir, K., Mooney, D.J., 2011. Active scaffolds for on-demand drug and cell delivery. Proc. Natl. Acad. Sci. 108, 67–72.